Elastic Moduli of Transversely Isotropic Graphite Fibers and Their Composites

Equations used to calculate the complete set of elastic
transversely isotropic properties for unidirectional fiber-reinforced materials
having transversely isotropic fibers are experimentally
verified by using improved ultrasonic techniques

by R.D. Kriz and W.W. Stinchcomb

ABSTRACT—This paper demonstrates that it is possible to
calculate the complete set of elastic mechanical properties for
graphite–epoxy fiber-reinforced materials at any fiber-volume
fraction by modifying equations previously developed to
include transversely isotropic graphite-fiber properties. Experi-
mental verification of the modified equations is demonstrated
by using these equations to curve fit elastic-property data
obtained ultrasonically over a range of fiber-volume fractions.
Material systems under consideration are T300/5208, AS-3501
and Modomor II/LY558 graphite epoxy. Using the modified
equations it is possible to extrapolate for fiber properties.
From Modomor II/LY558 ultrasonic data, it is shown that five
out of seven extrapolated graphite-fiber properties are
consistent with the assumption that graphite fibers are
transversely isotropic. Elastic properties for T300/5208 and
AS-3501 are ultrasonically evaluated by propagating stress
waves through six individual specimens cut at various angles
from a block of unidirectional material. Particular attention is
devoted to specimen dimensions. To demonstrate the need
for accurately calculating or experimentally measuring all
lamina elastic properties, a brief discussion is included on the
effect that variations in lamina elastic properties have on
calculating interlaminar stresses.

List of Symbols

A = unidirectional block dimensions, m
C_{ij} = material stiffnesses, contracted notation
  $(i,j = 1,2,3,4,5,6)$, Pa
c_i = wave-phase speeds $(i = 1,2,3)$, m/s
D = transducer diameter, m
E_i = Young's moduli along lamina coordinates
  $(i = 1,2,3)$, Pa

E_b = matrix Young's modulus, Pa
E_{f_L} = fiber longitudinal Young's modulus, Pa
E_{f_T} = fiber Young's modulus in the transverse plane, Pa
G_{ij} = shear moduli in the lamina i-j plane
  $(i,j = 1,2,3)$, Pa
G_b = matrix shear modulus, Pa
$G_{f_{LT}}$ = fiber shear modulus in the longitudinal–transverse
  plane, Pa
$G_{f_{TT}}$ = fiber shear modulus in the transverse plane, Pa
K_b = matrix plane-strain bulk modulus, Pa
$K_{f_{TT}}$ = fiber plane-strain bulk modulus, Pa
L = specimen length, m
M = margin, m
QL = quasi-longitudinal wave
QT = quasi-transverse wave
S = time separating QL and QT waves, s
T_{max} = specimen thickness necessary to separate QL and
  QT waves, m
T_{min} = specimen thickness satisfying energy-flux
  requirements, m
b = matrix-volume fraction
V_f = fiber-volume fraction
W = transmitted pulse width, s
θ = angular deviation of energy flow from the wave
  normal, deg
ν_b = matrix Poisson's ratio
$\nu_{f_{LT}}$ = fiber Poisson's ratio in the longitudinal–transverse
  plane
$\nu_{f_{TT}}$ = fiber Poisson's ratio in the transverse plane
ϱ = lamina mass density, kg/m³ (N-sec²/m⁴)

R.D. Kriz and W.W. Stinchcomb are Research Fellow and Associate
Professor, respectively, Department of Engineering Science and
Mechanics, Virginia Polytechnic Institute and State University, Blacksburg,
VA 24061.

Introduction

Several finite-element and finite-difference models
have been developed in order to predict the three-
dimensional stress distributions around holes or along a
free edge in various laminates. Most of the analytic
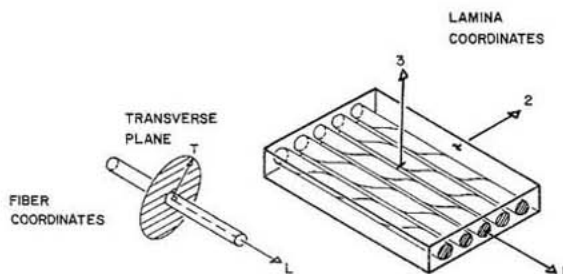finite-element and finite-difference models require nine

Fig. 1—Coordinate-system definition

independent elastic properties. Unfortunately, all nine properties representative of real materials are difficult to obtain; therefore, it is not uncommon to make simplifying approximations for material properties in order to obtain solutions.[1-3] It follows that more emphasis should be placed on accurately calculating or experimentally measuring all material properties if meaningful stress distributions are to be obtained by the various models.

Each laminate layer (lamina) is assumed to be constructed of fiber-reinforced materials, as shown in Fig. 1. When the fibrous lamina are assumed to be transversely isotropic, the number of independent material constants reduces to five. The five most commonly used independent engineering constants are listed below:

$$E_1, E_2, G_{12}, \nu_{12}, G_{23}$$

The symbols E, G and ν are Young's modulus, shear modulus and Poisson's ratio, respectively, and numbered subscripts refer to lamina coordinates, shown in Fig. 1.

For transversely isotropic materials, the Poisson's ratio in the 2-3 plane is related to E_2 and G_{23} by eq (1).*

$$\nu_{23} = E_2/2G_{23} - 1 \qquad (1)$$

Experimental measurement of G_{23} or ν_{23} is not as easily obtained as those of properties in the 1-2 plane. This has led some authors to use the approximations $G_{23} = G_{12}$ and $\nu_{23} = \nu_{12}$. Unfortunately, these approximations are not consistent with the transversely isotropic lamina properties shown below which were calculated from equations developed by Hashin[4] using isotropic glass-fiber properties at a fiber-volume fraction of 60 percent.

$G_{12}=0.640$ Msi (4.41 GPa), $G_{23}=0.726$ Msi (5.01 GPa)
$\nu_{12}=0.252$, $\nu_{23}=0.334$

Not all fiber-reinforced materials have isotropic fibers. Due to improved stiffness-to-weight and strength-to-weight ratios, most fiber-reinforced materials are constructed of boron or graphite fibers which are anisotropic. Whitney[5] suggested that all existing micro-mechanics analyses, which are intended for isotropic-fiber properties, can be easily adapted to take into account fiber anisotropy if the fibers are assumed to be transversely isotropic. Hashin[4] derived equations for calculating the complete set of transversely isotropic lamina properties such that either isotropic or transversely isotropic fiber properties
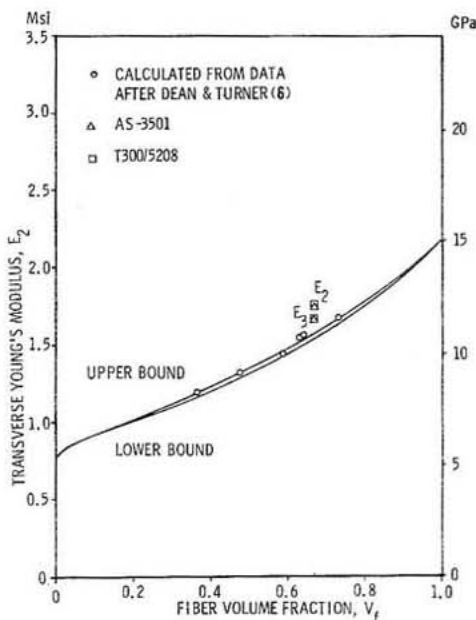
Fig. 2—Transverse Young's modulus, E_2

could be used. Unfortunately, the complete set of transversely isotropic fiber properties is difficult to measure due to the small fiber diameter. Using Hashin's equations, Dean and Turner[6] demonstrated that most of the transversely isotropic-graphite-fiber properties could be extrapolated for by curve-fitting ultrasonic data over a range of fiber volume fractions for Modmor II/LY558. Unfortunately, because of scatter in ultrasonic data, Dean and Turner were not able to extrapolate for all Modmor II graphite-fiber properties.
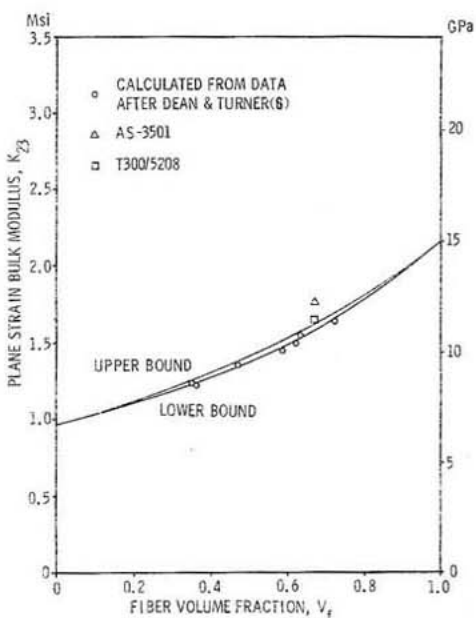

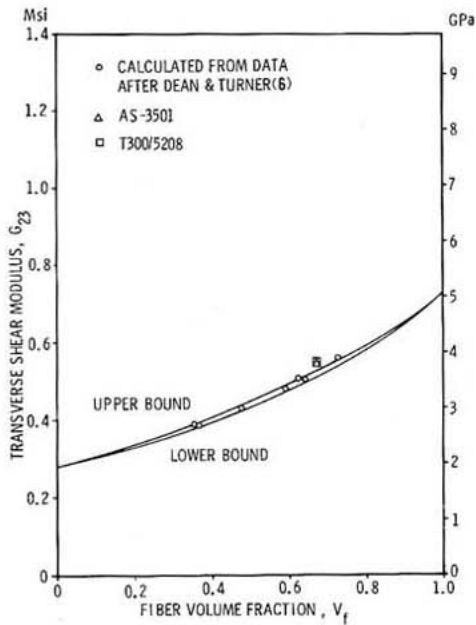Fig. 3—Plane-strain bulk modulus, K_{23}
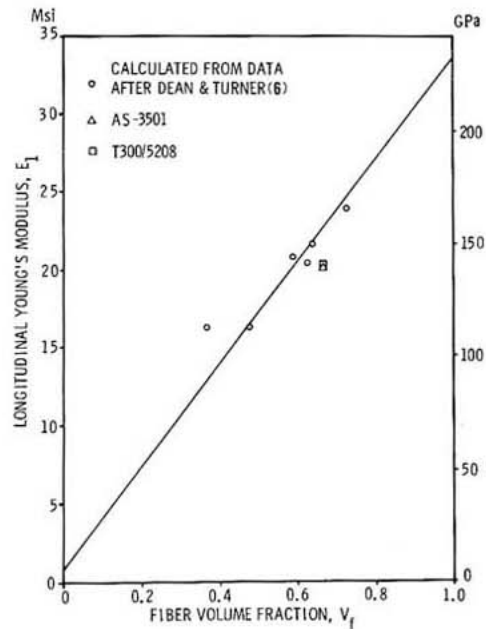
Fig. 4—Transverse-shear modulus, G_{23}

Fig. 6—Shear modulus in plane of fibers, G_{12}

This paper improves on the technique developed by Dean and Turner by demonstrating that the complete set of transversely isotropic properties can be obtained even though the ultrasonic data contain inherent scatter. This is done by curve fitting ultrasonic data using Hashin's modified equations written in terms of engineering elastic properties. Five out of seven curves fit the ultrasonic data well enough to extrapolate for fiber properties. For graphite fibers, the five extrapolated fiber properties are consistent with the assumption that fibers are transversely isotropic. Therefore, the remaining fiber properties need not be obtained by extrapolation but can be calculated from equations which were derived in Ref. 7 assuming transverse isotropy. With the complete set of fiber and matrix properties, Hashin's modified equations can now be used to calculate the complete set of transversely isotropic lamina elastic properties.
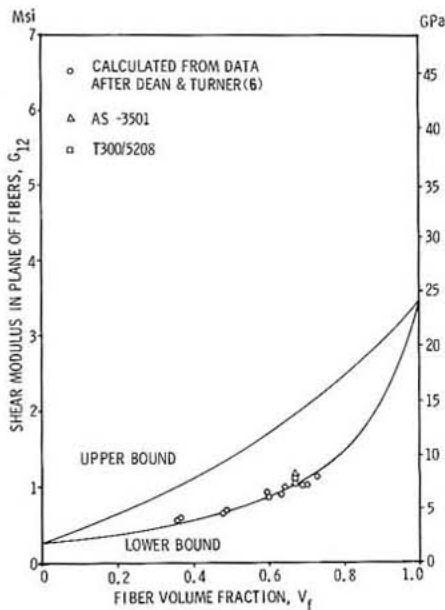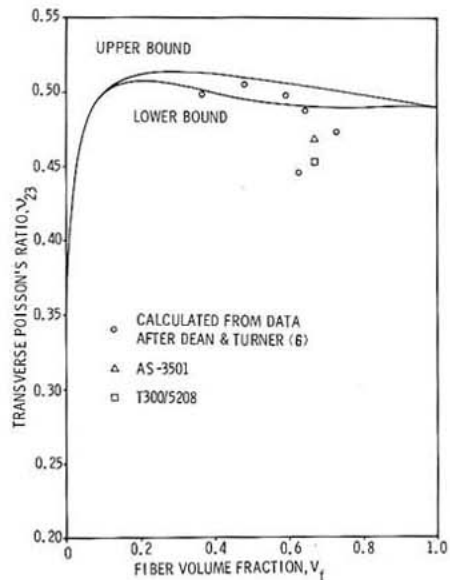

Fig. 5—Longitudinal Young's modulus, E_1

Fig. 7—Transverse Poisson's ratio, ν_{23}

TABLE 1—FIBER AND MATRIX PROPERTIES EXTRAPOLATED FROM FIGS. 2-8

	E_{f_L}	$\nu^*_{f_{LT}}$	$G_{f_{LT}}$	$G_{f_{TT}}$	$K_{f_{TT}}$	$E_{f_{TT}}$	$\nu^*_{f_{TT}}$
Modmor II Fiber (transversely isotropic)	33.7 Msi (232 GPa)	0.279	3.48 Msi (24.0 GPa)	0.728 Msi (5.02 GPa)	2.17 Msi (15.0 GPa)	2.17 Msi (15.0 GPa)	0.490

	E_b	ν_b
LY558 Epoxy Resin (isotropic)	0.7662 Msi ~~0.7762 Msi~~ (~~5.35 GPa~~) 5.28 GPa	0.354

* Fiber properties calculated from Eqs (2) and (3).

Extrapolating for Transversely Isotropic Fiber Properties

Equations developed by Hashin[4] are used to curve fit properties obtained over a range of fiber-volume fractions shown in Figs. 2-8. These equations are modified to include transversely isotropic fiber properties as suggested by Whitney.[5] A detailed development is given in Ref. 7. The necessary equations for curve fitting data shown in Figs. 2-8 are listed in the Appendix.

Dean and Turner[6] used the equations listed in the Appendix written in terms of stiffnesses to curve fit ultrasonic data obtained over a range of fiber-volume fractions. Although it may be more convenient to work in terms of stiffnesses when making ultrasonic measurements, physical interpretation of material properties is more meaningful when left in terms of engineering properties. Therefore, data obtained by Dean and Turner[6] were transformed into engineering properties and plotted in Figs. 2-8.
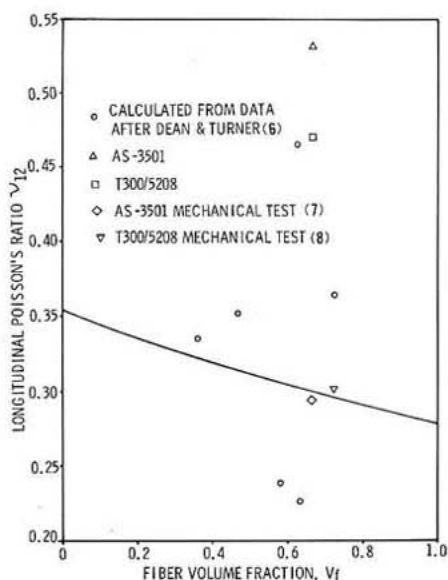
Modmor II fiber properties and LY558 epoxy-resin

Fig. 8—Longitudinal Poisson's ratio, ν_{12}

TABLE 2—PROPERTY-WAVE RELATIONS

Specimen No.	Wave Normal Direction Cosines	Particle Direction	Type of Wave	Equation Relating Elastic Moduli and Phase Velocity
1	$\nu_1 = 1$	X_1	L	$c_{11} = \rho c_1^2$
	$\nu_2 = 0$	X_2	T	$c_{66} = \rho c_2^2$
	$\nu_3 = 0$	X_3	T	$c_{55} = \rho c_3^2$
2	$\nu_1 = 0$	X_1	T	$c_{66} = \rho c_1^2$
	$\nu_2 = 1$	X_2	L	$c_{22} = \rho c_2^2$
	$\nu_3 = 0$	X_3	T	$c_{44} = \rho c_3^2$
3	$\nu_1 = 0$	X_1	T	$c_{55} = \rho c_1^2$
	$\nu_2 = 0$	X_2	T	$c_{44} = \rho c_2^2$
	$\nu_3 = 1$	X_3	L	$c_{33} = \rho c_3^2$
4	$\nu_1 = 0$	X_1	T	$c_{66} + c_{55} = 2\rho c_1^2$
	$\nu_2 = 1/\sqrt{2}$	X_2X_3 Plane	L	$c_{23} = \sqrt{(c_{22} + c_{44} - 2\rho c_2^2)(c_{44} + c_{33} - 2\rho c_2^2)} - c_{44}$
	$\nu_3 = 1/\sqrt{2}$	X_2X_3 Plane	T	$c_{23} = \sqrt{(c_{22} + c_{44} - 2\rho c_2^2)(c_{44} + c_{33} - 2\rho c_3^2)} - c_{44}$
5	$\nu_1 = 1/\sqrt{2}$	X_1X_3 Plane	QL	$c_{13} = \sqrt{(c_{11} + c_{55} - 2\rho c_2^2)(c_{55} + c_{33} - \rho^2 c_2^2)} - c_{55}$
	$\nu_2 = 0$	X_2	T	$c_{66} + c_{44} = 2\rho c_1^2$
	$\nu_3 = 1/\sqrt{2}$	X_1X_3 Plane	QT	$c_{13} = \sqrt{(c_{11} + c_{55} - 2\rho c_3^2)(c_{55} + c_{33} - 2\rho c_3^2)} - c_{55}$
6	$\nu_1 = 1/\sqrt{2}$	X_1X_2 Plane	QL	$c_{12} = \sqrt{(c_{11} + c_{55} - 2\rho c_2^2)(c_{66} + c_{22} - 2\rho c_2^2)} - c_{66}$
	$\nu_2 = 1/\sqrt{2}$	X_1X_2 Plane	QT	$c_{12} = \sqrt{(c_{11} + c_{66} - 2\rho c_3^2)(c_{66} + c_{22} - 2\rho c_3^2)} - c_{66}$
	$\nu_3 = 0$	X_3	T	$c_{55} + c_{44} = 2\rho c_1^2$

Fig. 9—Energy-flux deviation in the X_1-X_2 and X_1-X_3 planes
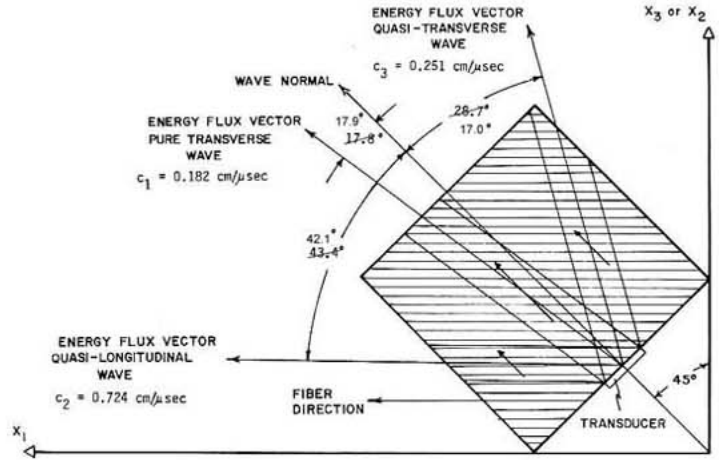
properties, listed in Table 1, were extrapolated for as shown in Figs. 2-6 using eqs (11)-(15).

Two improvements in the extrapolation technique originally developed by Dean and Turner[6] are realized in this paper. First, as suggested by Hashin,[4] the lamina properties E_2 and G_{23} are more closely represented by the upper bound equations which were used to extrapolate for fiber properties E_{f_T} and G_{f_T}. Second, the extrapolation of $\nu_{f_{LT}}$ and $\nu_{f_{TT}}$ is not necessary. If the transverse plane of the fiber is assumed to be isotropic, then, as shown in Ref. 7, $\nu_{f_{LT}}$ and $\nu_{f_{TT}}$ may be calculated from the other extrapolated fiber properties using eqs (2) and (3).

$$\nu_{f_{LT}} = \sqrt{E_{f_L}(2K_{f_{TT}} - E_{f_T} - 2K_{f_{TT}}\nu_{f_{TT}})/4K_{f_{TT}}E_{f_T}}$$
(2)

$$\nu_{f_{TT}} = E_{f_T}/2G_{f_{TT}} - 1$$
(3)

Curves drawn in Figs. 7 and 8 do not curve fit data but are calculated from eqs (16) and (17) using fiber properties calculated from eqs (2) and (3), respectively.

Ultrasonic Evaluation of Lamina Properties

Elastic lamina properties were ultrasonically evaluated by measuring the phase velocities of longitudinal and shear waves propagating through the material at various angles with respect to the lamina coordinates. Depending on the direction cosines, ν_i, chosen for the wave normal, a sufficient number of equations are obtained which relate stiffness components, C_{ij}, and wave-phase velocities, c_i. All equations relevant to the determination of material

stiffnesses from the wave phase speeds are derived in Ref. 7 and listed in Table 2.

It is usually assumed that the energy of the plane wave propagates in the same direction as the wave normal. Unfortunately, in some materials, the deviation between the direction of the energy propagation (energy-flux vector) and the wave normal may be as large as 40 deg. If thick specimens are used to experimentally determine the wave-phase speeds, the direction of the propagating energy should be calculated in order to assure the experimentalist that the propagating wave is not reflecting off unexpected boundaries, as shown in Fig. 9. Equations used to calculate these angles are derived in Ref. 7, but are too lengthy to be included in this paper.

An example of the deviation in the directions between the energy-flux vector and wave normal is demonstrated by utilizing graphite/epoxy properties listed in Table 3 which were obtained from data curve fitted in Figs. 2-8. Using the stiffness properties listed in Table 3, the deviation of the energy-flux vector from the wave normal is calculated using equations developed in Ref. 7. The results are listed in Table 4.

Of particular interest are Specimens 5 and 6, since the particle displacements are neither parallel nor perpendicular to the wave normal. Therefore, these waves have been labeled as quasi-longitudinal (QL) and quasi-transverse (QT) depending on whether the largest component of the particle displacement is parallel or perpendicular to the wave normal. Using information listed in Table 4, graphical demonstration of the deviation of the energy-flux vector from the wave normal is shown in Fig. 9.

As can be seen in Fig. 9, the deviation in the energy-

TABLE 3—ENGINEERING AND STIFFNESS PROPERTIES OBTAINED FROM CURVE-FITTING ULTRASONIC DATA, FIGS. 2-8

Lamina Properties at a Fiber-volume Fraction of 0.67

C_{11} = 23.4 Msi (161 GPa)	E_1 = 22.8 Msi (157 GPa)
$C_{22} = C_{33}$ = 2.10 Msi (14.5 GPa)	$E_2 = E_3$ = 1.57 Msi (10.8 GPa)
$C_{12} = C_{13}$ = 0.943 Msi (6.50 GPa)	$\nu_{12} = \nu_{13}$ = 0.300
C_{23} = 1.05 Msi (7.24 GPa)	ν_{23} = 0.489
C_{44} = 0.527 Msi (3.63 GPa)	G_{23} = 0.527 Msi (3.63 GPa)
$C_{55} = C_{66}$ = 1.03 Msi (7.10 GPa)	$G_{12} = G_{13}$ = 1.03 Msi (7.10 GPa)
ϱ = 0.151 × 10⁻³ lb$_f$-s²/in.⁴ (1.61 × 10⁻⁵ N-s²/cm²)	

flux vector for the QL and QT waves should not be ignored when determining the size of the specimens to be tested. Other variables such as transducer size, separation of QL and QT waves, maximum pulse width, and material attenuation must also be considered in sizing specimens.

The size of the specimens was also limited by the size of the block from which they were cut. The specimens were cut from a block of unidirectional graphite/epoxy as shown in Fig. 10. Except for Specimens 5 and 6, the direction of the energy-flux vector is coincident with the wave normal. Both Specimens 5 and 6 are cut at 45 deg to the fiber direction, as shown in Fig. 11. These specimens must be sufficiently thin so that the energy flux propagated
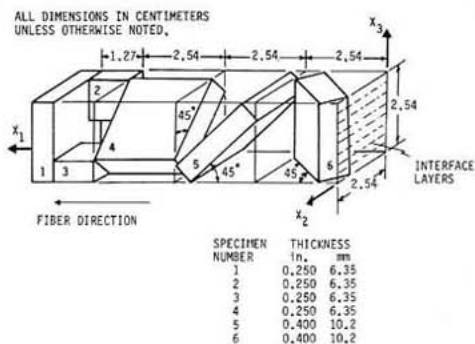

ALL DIMENSIONS IN CENTIMETERS UNLESS OTHERWISE NOTED.

SPECIMEN NUMBER	THICKNESS in.	mm
1	0.250	6.35
2	0.250	6.35
3	0.250	6.35
4	0.250	6.35
5	0.400	10.2
6	0.400	10.2

Fig. 10—Specimen dimensions

TABLE 4—DEVIATION OF ENERGY-FLUX DIRECTION FROM WAVE NORMAL

| Specimen No.	Wave Normal Direction Cosines	Particle Direction	Type of Wave	Deviation of Energy Flux Vector Direction From Wave Normal θ degrees
1	$\nu_1 = 1$	x_1	L	0
	$\nu_2 = 0$	x_2	T	0
	$\nu_3 = 0$	x_3	T	0
2	$\nu_1 = 0$	x_1	T	0
	$\nu_2 = 1$	x_2	L	0
	$\nu_3 = 0$	x_3	T	0
3	$\nu_1 = 0$	x_1	T	0
	$\nu_2 = 0$	x_2	T	0
	$\nu_3 = 1$	x_3	L	0
4	$\nu_1 = 0$	x_1	T	0
	$\nu_2 = 1/\sqrt{2}$	$x_2 x_3$ Plane	L	0
	$\nu_3 = 1/\sqrt{2}$	$x_2 x_3$ Plane	T	0
5	$\nu_1 = 1/\sqrt{2}$	$x_1 x_3$ Plane	QL	~~43.4~~ 42.1
	$\nu_2 = 0$	x_2	T	~~17.8~~ 17.9
	$\nu_3 = 1/\sqrt{2}$	$x_1 x_3$ Plane	QT	~~28.7~~ 17.0
6	$\nu_1 = 1/\sqrt{2}$	$x_1 x_2$ Plane	QL	~~43.4~~ 42.1
	$\nu_2 = 1/\sqrt{2}$	$x_1 x_2$ Plane	QT	~~28.7~~ 17.0
	$\nu_3 = 0$	x_3	T	~~17.8~~ 17.9
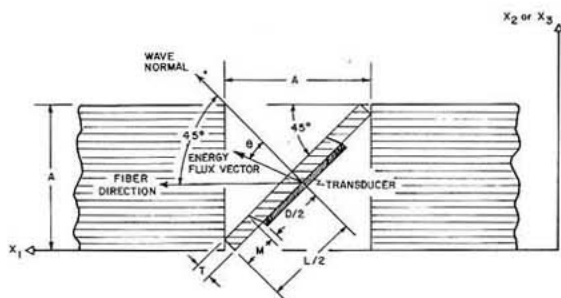
Fig. 11—Influence of energy-flux deviation on dimensions for specimen Nos. 5 and 6
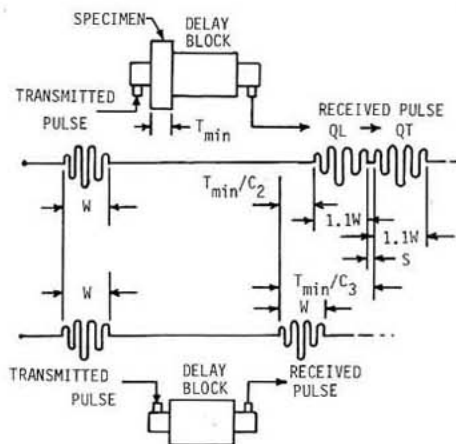
Fig. 12—Separation of QL and QT waveforms

by a transducer of diameter D is not received as a reflection from some other surface. As shown in Fig. 11, the maximum allowable thickness, T_{max}, can be calculated from eq (4) given the dimensions of the block, A, margin, M, transducer diameter, D, and angular deviation of the energy flow from the wave normal, θ.

$$T_{max} = \frac{A - (2M + D) \cos 45}{2 \tan \theta \cos 45 + \cos 45} \qquad (4)$$

As shown in Fig. 12, these specimens must also be sufficiently thick to allow separation of the QL and QT

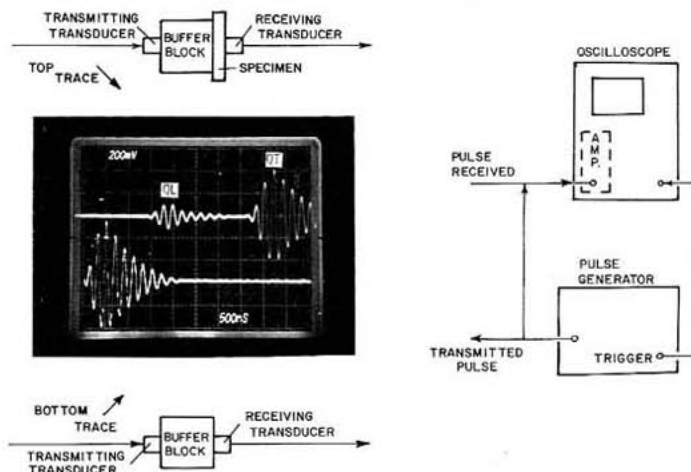Fig. 13—Ultrasonic apparatus and sample waveform

waves. The minimum allowable thickness, T_{min}, can be calculated from eq (5):

$$T_{min} = \frac{(1.1\ W + S)\ c_2 c_3}{c_2 - c_3} \tag{5}$$

The final allowable thickness, T, must satisfy inequality (6) if both energy-flux deviation and wave-separation requirements are to be satisfied.

$$T_{min} \le T \le T_{max} \tag{6}$$

Using the properties listed in Tables 3 and 4, maximum and minimum thicknesses for Specimens 5 and 6 are calculated and listed below, given $A = 1.0$ in. (2.54 cm), $M = 0.05$ in. (0.127 cm), $D = 0.25$ in. (0.635 cm), $S = 0.1\ \mu s$, and $W = 2.25\ \mu s$.

$T_{min} = 0.389$ in. (0.988 cm), $T_{max} = 0.403$ in. (1.02 cm)

Since the maximum thickness for Specimens 5 and 6 is only 1.02 cm, the pulse-echo technique could not be used because the time duration between echoes would be less than the initial pulse width. Therefore, the send–receive technique with a fused-silica delay block was used as shown in Fig. 13. For Specimens 1 through 4, no deviation in energy flux was calculated. Therefore, the only restriction on thickness for these specimens is that the thickness be large enough for accurate wave-speed measurement but small enough so that the received pulse is not completely attenuated. Final dimensions for Specimens 1 through 6 are shown in Fig. 10.
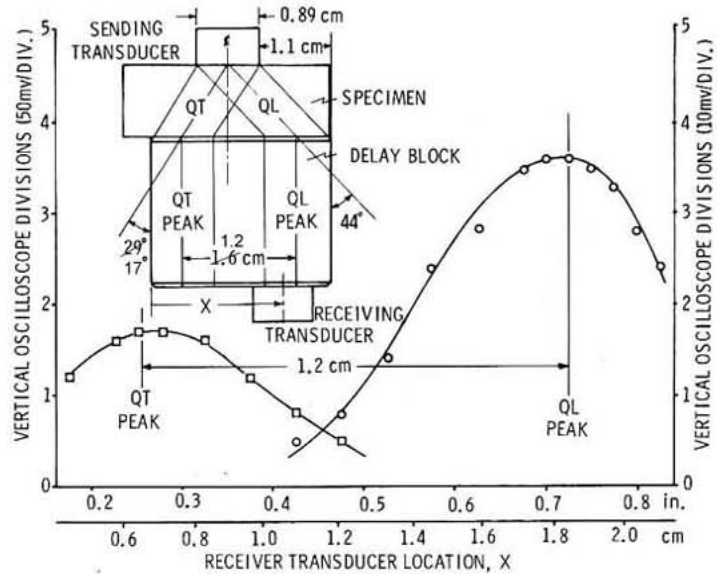
Experimental Procedure

The experimental material stiffness properties, C_{ij} are calculated from equations listed in Table 2 where the wave-phase speed is determined experimentally. Panametric transducers M110 and V156 were used to propagate longitudinal and shear waves, respectively, at a frequency of 5 MHz by using a Matec pulse generator (Model 6000) with a 1 MHz-20 MHz R.F. plug-in (Model 755). A fused-quartz delay block was bonded to the specimen using phenyl salicylate.

The wave-phase speed was determined by first measuring the time required for a group of stress waves to travel through the delay block and graphite–epoxy specimen. A second measurement was made to determine the time required for the same group of stress waves to travel through the delay block. Sample traces from the oscilloscope, showing the stress waves traveling through the block-specimen combination (upper trace) and the stress waves traveling through the delay block (lower trace), are shown in Fig. 13. The difference in time between the two received signals is the time required for the group stress waves to travel through the specimen. Therefore, the velocity can be calculated given the specimen thickness. Time measurements between the two received signals were taken from the maximum peak of each envelope.

TABLE 5—EXPERIMENTAL STIFFNESS PROPERTIES

Specimen No.	Wave Normal Direction Cosine	Displacement Direction	Wave Type	AS-3501					T300/5208				
				Wave Speed cm/µsec	Experimental Stiffness GPa	Symbol	Predicted Stiffness GPa $V_f=0.67$	Percent Difference	Wave Speed cm/µsec	Experimental Stiffness GPa	Symbol	Predicted Stiffness GPa $V_f=0.67$	Percent Difference
1	$\nu_1=1$	x_1	L	0.974	153	c_{11}	161	5	0.987	154	c_{11}	161	4
	$\nu_2=0$	x_2	T	0.224	8.10	c_{66}	7.10	14	0.223	7.84	c_{66}	7.10	10
	$\nu_3=0$	x_3	T	0.224	8.10	c_{55}	7.10	14	0.223	7.84	c_{55}	7.10	10
2	$\nu_1=0$	x_1	T	0.230	8.54	c_{66}	7.10	20	0.223	7.84	c_{66}	7.10	10
	$\nu_2=1$	x_2	L	0.319	16.4	c_{22}	14.5	13	0.315	15.7	c_{22}	14.5	8
	$\nu_3=0$	x_3	T	0.164	4.31	c_{44}	3.63	19	0.162	4.14	c_{44}	3.63	14
3	$\nu_1=0$	x_1	T	0.212	7.26	c_{55}	7.10	2	0.223	7.84	c_{55}	7.10	10
	$\nu_2=0$	x_2	T	0.156	3.90	c_{44}	3.63	7	0.160	4.05	c_{44}	3.63	12
	$\nu_3=1$	x_3	L	0.311	15.6	c_{33}	14.5	7	0.308	15.0	c_{33}	14.5	3
4	$\nu_1=0$	x_1	T	0.217	15.2	$c_{66}+c_{55}$	14.2	7	0.223	16.1	$c_{66}+c_{55}$	14.2	13
	$\nu_2=1/\sqrt{2}$	$x_2 x_3$ Plane	L	0.308	6.70	c_{23}	7.24	4	0.314	7.58	c_{23}	7.24	5
	$\nu_3=1/\sqrt{2}$	$x_2 x_3$ Plane	T	0.158	7.91	c_{23}	7.24	9	0.161	7.10	c_{23}	7.24	2
5	$\nu_1=1/\sqrt{2}$	$x_2 x_3$ Plane	QL	0.680	*	c_{13}	6.50	-	0.707	*	c_{13}	6.50	-
	$\nu_2=0$	x_2	T	0.192	11.9	$c_{66}+c_{44}$	10.7	11	0.196	12.2	$c_{66}+c_{44}$	10.7	14
	$\nu_3=1/\sqrt{2}$	$x_1 x_3$ Plane	QT	No Data	-	c_{13}	6.50	-	0.260	6.96	c_{13}	6.50	7
6	$\nu_1=1/\sqrt{2}$	$x_1 x_2$ Plane	QL	0.679	*	c_{12}	6.50	-	0.685	*	c_{12}	6.50	-
	$\nu_2=1/\sqrt{2}$	$x_1 x_2$ Plane	QT	0.266	13.3	c_{12}	6.50	104	0.261	9.09	c_{12}	6.50	40
	$\nu_3=0$	x_3	T	0.192	11.8	$c_{55}+c_{44}$	10.7	10	0.197	12.3	$c_{55}+c_{44}$	10.7	15

* Imaginary

Fig. 14—Geometrix separation of QL and QT waves

Results and Discussion

Using the experimental procedure previously described, the material-stiffness properties were obtained for AS-3501 and T300/5208 graphite–epoxy specimens. The experimental results are listed in Table 5 and compared with the material stiffnesses calculated from properties obtained at the same fiber-volume fraction from the curve fit shown in Figs. 2-8.

It is interesting to note that several different values occur for C_{44}, C_{55} and C_{66}. This variation is most likely due to nonuniformity of fiber-volume fraction and density in the block from which the specimens were cut. Therefore, those experimental stiffnesses which compared best with the predicted stiffnesses were used in the formulas, shown in Table 2, to calculate values for C_{23}, C_{13} and C_{12}. Similarly, only those experimental stiffnesses which were closest to predicted stiffnesses were used to calculate the corresponding engineering properties which were plotted in Figs. 2-8.

As shown in Table 5, all stiffnesses except C_{12} and C_{13} compare reasonably well with those predicted. Values calculated for C_{12} and C_{13} from equations listed in Table 2 are extremely sensitive to the accuracy to which the wave-phase speed, c_i, is measured. A 0.1-percent variation in measuring wave-phase speed will cause a 35-percent variation in values of C_{12} and C_{13} calculated from properties listed in Table 3. Therefore, if the stiffnesses C_{12} and C_{13} are to be obtained within five-percent accuracy, at least five places of accuracy must be measured for all wave speeds and stiffnesses used in the calculation. However, local variations in specimen density and fiber volume, along with errors introduced by measuring distances on an oscilloscope trace, eliminate any possibility of realistically measuring the wave speeds with the required accuracy. As shown in Figs. 7 and 8, engineering properties v_{23} and v_{12} are most affected, since C_{12} and C_{13} appear as the dominating terms in the numerator of eqs (7) and (8).

$$v_{12} = \frac{C_{12}C_{33} - C_{23}C_{13}}{C_{22}C_{33} - C_{23}{}^2} \qquad (7)$$

$$v_{23} = \frac{C_{11}C_{23} - C_{12}C_{13}}{C_{11}C_{33} - C_{13}{}^2} \qquad (8)$$

Fortunately, the data scatter shown in Figs. 7 and 8 has no effect on obtaining the complete set of transversely isotropic fiber properties. As shown in Figs. 2-6, five fiber properties are independently obtained by fitting Hashin's equations to ultrasonic data. Transverse isotropy is demonstrated by taking any of the four extrapolated fiber properties and calculating the fifth. Additional verification is demonstrated by plotting mechanical data for v_{12} on Fig. 8 where the curve was calculated from eq (14) which used a value for $v_{f_{LT}}$ calculated from eq (2). Therefore, accurate measurement of C_{12} or C_{13} is not necessary if transversely isotropic properties are to be obtained for the material system under investigation. The investigator only needs to extrapolate for the five fiber properties shown in Figs. 2-6 and use eqs (2) and (3), along with equations listed in the Appendix, to obtain the complete set of transversely isotropic lamina properties.

Conclusions

A complete set of elastic constants may be obtained for graphite-/epoxy-composite laminae using the equations of Hashin along with values of properties for transversely isotropic fibers and the matrix material. The calculated elastic constants are in good agreement with values obtained from ultrasonic velocity measurements. In making the experimental measurements, special attention was given to deviation between the energy-flux vector and the wave normal which was as large as 43 deg in some cases. The quasi-longitudinal and quasi-transverse waves which occur in this situation are of particular interest and sample waveforms are shown in Fig. 13. As shown in the top trace of Fig. 13, the QT wave is of much larger magnitude than the QL wave. The magnitude of the QL and QT waves can be varied depending on the location of the receiving transducer. The geometric separation of QL and QT waves is graphically demonstrated in Fig. 14

using angles listed in Table 4, and the relative magnitude of QL and QT waves is also shown. Although the distance measured between peaks of QL and QT waves is not exactly the same as predicted by theory, the general trend of energy-flux deviation is as predicted.

The assumption that a single lamina of graphite epoxy is transversely isotropic may not be completely valid when the plies are stacked and cured to form a multi-layered composite. Ultrasonic data are sensitive to the interfaces, and can be used as a measure of the quality of the interlaminar bonds.

Having obtained the complete set of lamina elastic properties, it is possible to demonstrate the effect that the approximations (9) and (10) have on the analytic three-dimensional stress distributions around holes or free edges in composite laminates.

$$G_{23} \approx G_{12} \approx G_{13} \qquad (9)$$

$$\nu_{23} \approx \nu_{12} \approx \nu_{13} \qquad (10)$$

Although several finite-element and finite-difference models may be used to demonstrate this property dependence, the perturbation solution developed by Hsu and Herakovich[3] is particularly attractive for such a parametric study since it is a closed form solution. In Ref. 9, a complete parametric study demonstrates the effect that variations and approximations of material properties, used in this paper, have on the interlaminar stress distributions in a $[\pm 45°]_s$ graphite-epoxy laminate. In particular, the distribution of interlaminar normal and shear stresses is sensitive to G_{23} and the free-edge interlaminar stresses, calculated using the properties presented in this paper, are greater than those calculated using approximations (9) and (10).

Acknowledgments

References

1. Pipes, R.B. and Pagano, N.J., "Interlaminar Stresses in Composite Laminates Under Uniform Axial Extension," J. of Comp. Mats., 4, 204 (1970).

2. Rybicki, E.F. and Schmueser, D.W., "Three Dimensional Finite Element Stress Analysis of Laminated Plates Containing a Circular Hole," AFML-TR-76-92 (Aug. 1976).

3. Hsu, P.W. and Herakovich, C.T., "A Perturbation Solution for Interlaminar Stresses in Composite Laminates," Composite Materials Testing and Design (Fourth Conference), ASTM STP 617, 296 (1977).

4. Hashin, Z., "Theory of Fiber Reinforced Materials," NASA-CR-1974 (Mar. 1972).

5. Whitney, J.M., "Elastic Moduli of Unidirectional Composites with Anisotropic Filaments," J. of Comp. Mats., 1, 188 (1967).

6. Dean, G.D. and Turner, P., "The Elastic Properties of Carbon Fibers and Their Composites," Composites (Jul. 1973).

7. Kriz, R.D. and Stinchcomb, W.W., "Mechanical Properties for Thick Fiber Reinforced Composite Materials Having Transversely Isotropic Fibers," VPI-E-77-13 (May 1977).

8. Hofer, Jr., K.E., Larsen, D. and Humphreys, V.E., "Development of Engineering Data on the Mechanical and Physical Properties of Advanced Composite Materials," NTIS #AD-A014 363 (Feb. 1975).

9. Kriz, R.D., "Effect of Material Properties on Interlaminar Stresses in Angle-Ply Composite Laminates," VPI-E-77-16, Virginia Polytechnic Institute and State University, Blacksburg, VA (1977).

APPENDIX

Equations developed by Hashin[4] are listed in terms of fiber and matrix properties denoted by subscripts f and b, respectively. The fiber properties are further denoted by subscripts L and T which correspond to the longitudinal and transverse fiber coordinates defined in Fig. 1. Fiber and matrix-volume fractions are denoted by V_f and V_b.

The upper and lower bounds for the plane-strain bulk modulus in the 2-3 plane shown in Fig. 1 are given as

$$K_{23}^{(-)*} = K_b + \cfrac{V_f}{\cfrac{1}{K_{f_{TT}} - K_b} + \cfrac{V_b}{K_b + G_b}} \qquad (a)$$

$$\qquad (11)$$

$$K_{23}^{(+)} = K_{f_{TT}} + \cfrac{V_b}{\cfrac{1}{K_b - K_{f_{TT}}} + \cfrac{V_f}{K_{f_{TT}} + G_{f_{TT}}}} \qquad (b)$$

where * indicates the equation used for curve fitting and the $(+)$ and $(-)$ signs indicate upper and lower bounds, respectively.

The remaining equations are written using similar notation.

$$G_{23}^{(-)} = G_b + \cfrac{V_f}{\cfrac{1}{G_{f_{TT}} - G_b} + \cfrac{V_b(K_b + 2G_b)}{2G_b(K_b + G_b)}} \qquad (a)$$

$$\qquad (12)$$

$$G_{23}^{(+)*} = G_b \frac{(1 + \alpha_1 V_f^3)(\alpha_2 + \beta_1 V_f) - 3 V_f V_b^2 \beta_1^2}{(1 + \alpha_1 V_f^3)(\alpha_2 - V_f) - 3 V_f V_b^3 \beta_1^2} \qquad (b)$$

where

$$\alpha_1 = \frac{\beta_1 - \gamma\beta_2}{1 + \gamma\beta_2}, \quad \beta_1 = \frac{1}{3 - 4\nu_b}, \quad \beta_2 = \frac{1}{3 - 4\nu_{f_{TT}}}$$

$$\beta_2 = \frac{K_{f_{TT}}}{K_{f_{TT}} + 2G_{f_{TT}}}$$

$$\alpha_2 = \frac{\gamma + \beta_1}{\gamma - 1}, \quad \text{and } \gamma = G_{f_{TT}}/G_b$$

$$G_{12}^{(-)*} = G_b + \cfrac{V_f}{\cfrac{1}{G_{f_{LT}} - G_b} + \cfrac{V_b}{2G_b}} = G_{13} \qquad (a)$$

$$\qquad (13)$$

$$G_{12}^{(+)} = G_{f_{LT}} + \cfrac{V_b}{\cfrac{1}{G_b - G_{f_{LT}}} + \cfrac{V_f}{2G_{f_{LT}}}} \qquad (b)$$

$$E_1 = V_f E_{f_L} + V_b E_b \qquad (14)$$

$$E_2 = E_3 = \frac{4K_{23}^{(-)*} G_{23}^{(-)*}}{K_{23}^{(-)*} + \Psi G_{23}^{(-)*}} \qquad (15)$$

$$\nu_{12} = \frac{V_f E_{f_L} L_1 + V_b E_b L_2 \nu_b}{V_f E_{f_L} L_3 + V_b E_b L_2} \qquad (16)$$

$$\nu_{23} = \nu_{32} = \frac{K_{23}^{(-)*} - \Psi G_{23}^{(-)*}}{K_{23}^{(-)*} + \Psi G_{23}^{(-)*}} \qquad (17)$$

where

$$\Psi = 1 + 4K_{23}^{(-)*} \nu_{12}^2 / E_1$$

$$L_1 = 2\nu_{f_{LT}}(1 - \nu_b^2) V_f + V_b(1 + \nu_b)\nu_b$$

$$L_2 = V_f(1 - \nu_{f_{LT}} - 2\nu_{f_{LT}}^2)$$

$$L_3 = 2(1 - \nu_b^2) V_f + (1 + \nu_b) V_b$$

ERRATA

J. EXP. MECHANICS, VOL.19, PP.41-49.

NOVENBER 24, 1987

R.D. KRIZ

Please note the following corrections:

1. Table 1. Change: E_b=0.7762 to E_b=0.7662.

2. Table 4. Change: 43.4° to 42.1°, 17.8° to 17.9°, and 28.7° to 17.0°.

3. Fig. 9. Change: 43.4° to 42.1°, 17.8° to 17.9°, and 28.7° to 17.0°.

4. Fig. 14. Change: 1.6 cm to 1.2 cm and 29° to 17°.

5. Appendix A: Change: $\beta_2 = 1/(3-4\nu_{f_{tt}})$ to $\beta_2 = K_{f_{tt}}/(K_{f_{tt}}+2G_{f_{tt}})$

Material properties plotted in Fig.s 2-7 which depend on E_b and β_2 differ by less than 1% when using the correct matrix and fiber properties listed Table 1. The corrections stated above have no effect on the extrapolated fiber properties. Therefore all of our conclusions are unaltered. Although these corrections are not numerically significant for the Gr/Ep material system evaluated here, there could be other fiber/matrix materials for which these corrections could be significant.